2026 International Conference on Green Aviation
Xi'an, November 1–3, 2026

Numerical Study of Unsteady Aerodynamics of Particles in Compressible Flows

Pavel Utkin

Harbin Institute of Technology
School of Astronautics
Department of Astronautical Science and Mechanics
International Center for Applied Mechanics

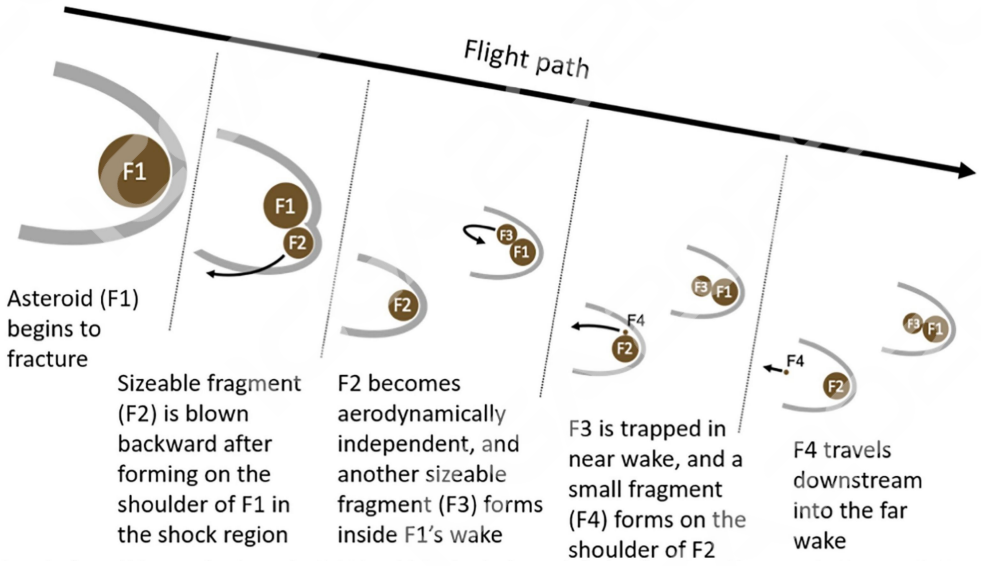
Email: utkin@hit.edu.cn



Introduction

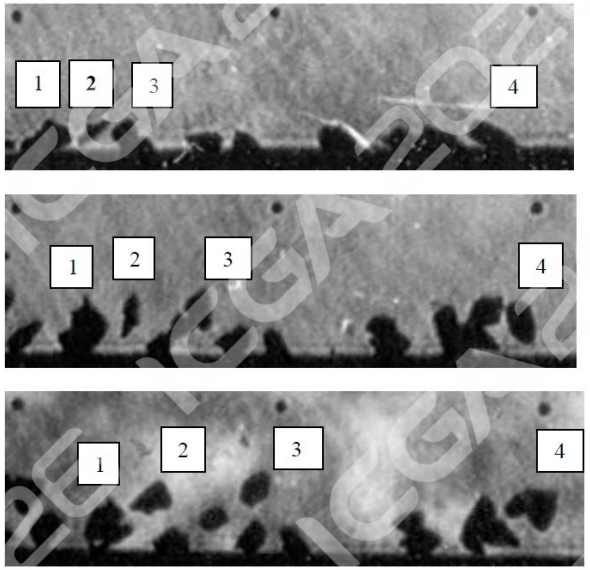
Modeling of the dynamics of one or multiple particles or bodies moving within high-speed compressible media

Aerodynamic behavior of meteoroid fragments traversing the atmosphere



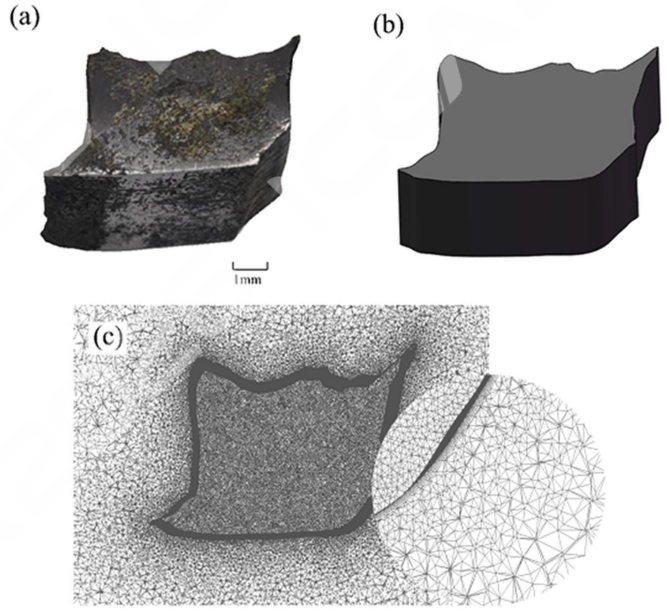
Register P.J. et al. // Icarus. 2020.

Transport of organic dust particle



Poplavski S.V. // J. Phys.: Conf. Ser. 2018. 1128.

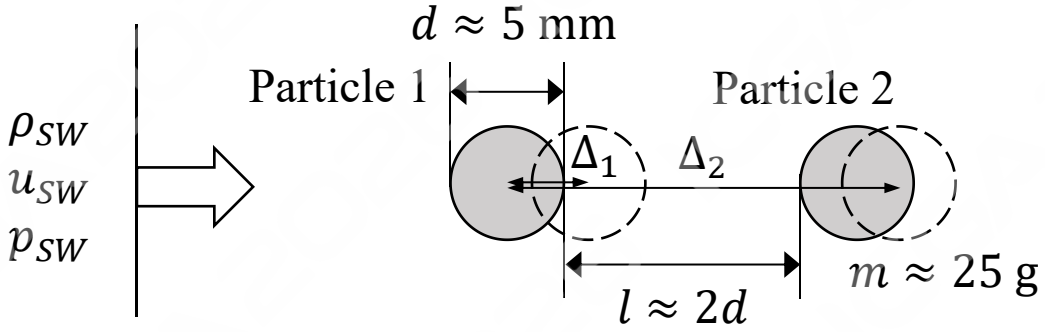
Evaluation of hazards associated with debris ejected during accidental explosions



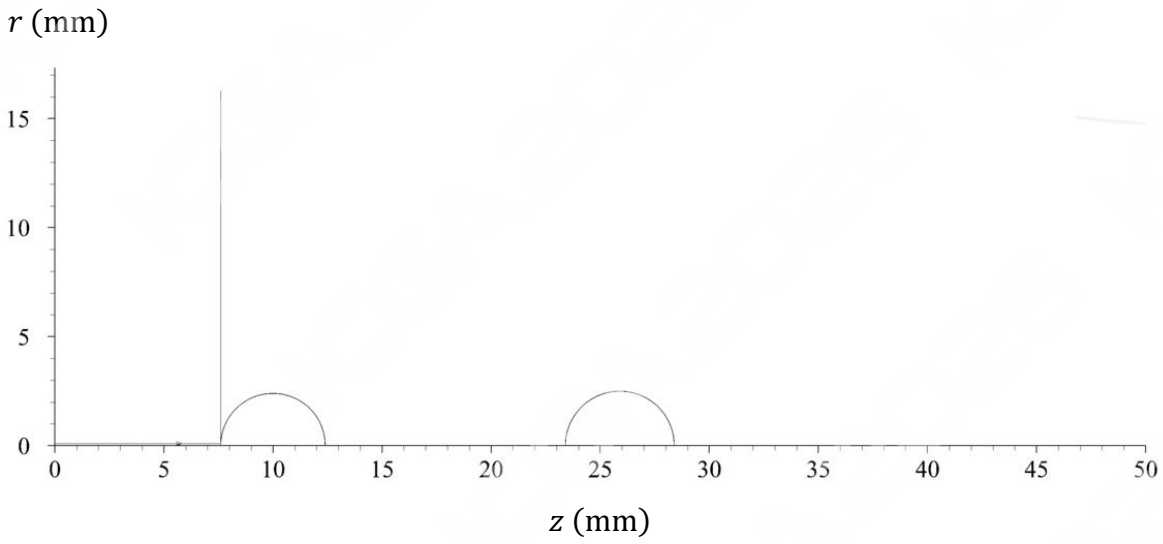
Xin D. et al. // Powder Tech. 2022.

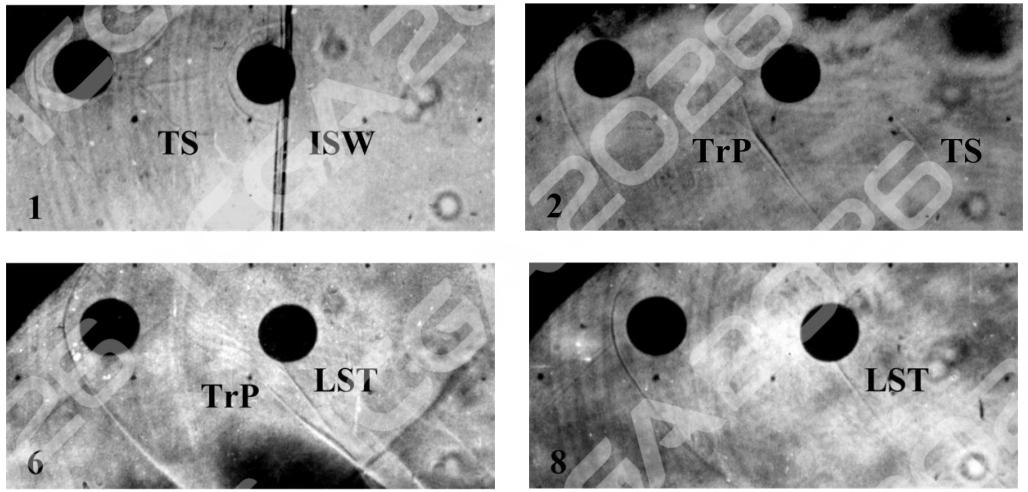
Introduction

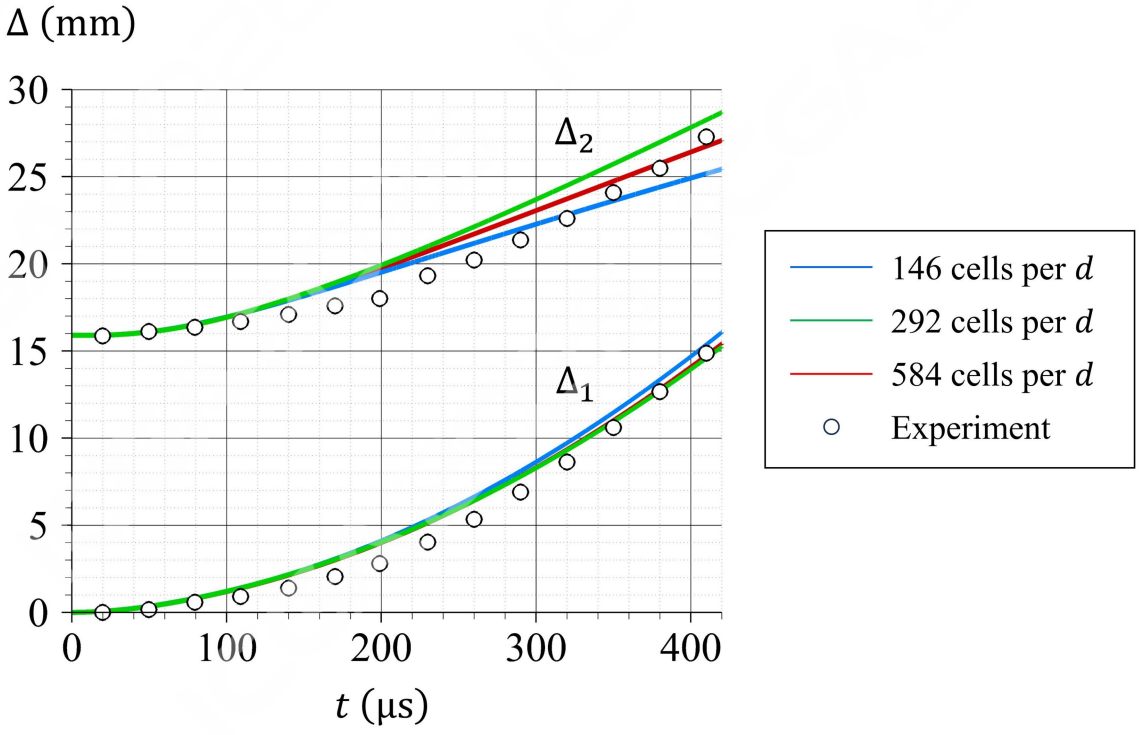
Unsteady aerodynamic effects



Shock wave, $M = 3.0$



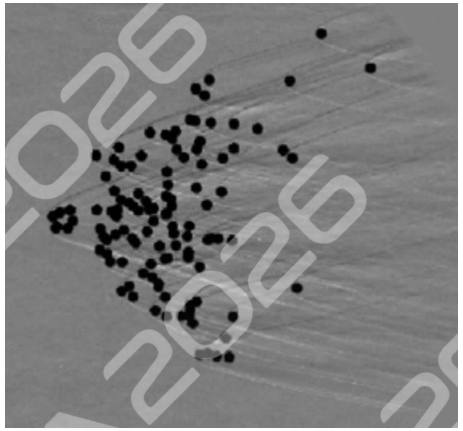




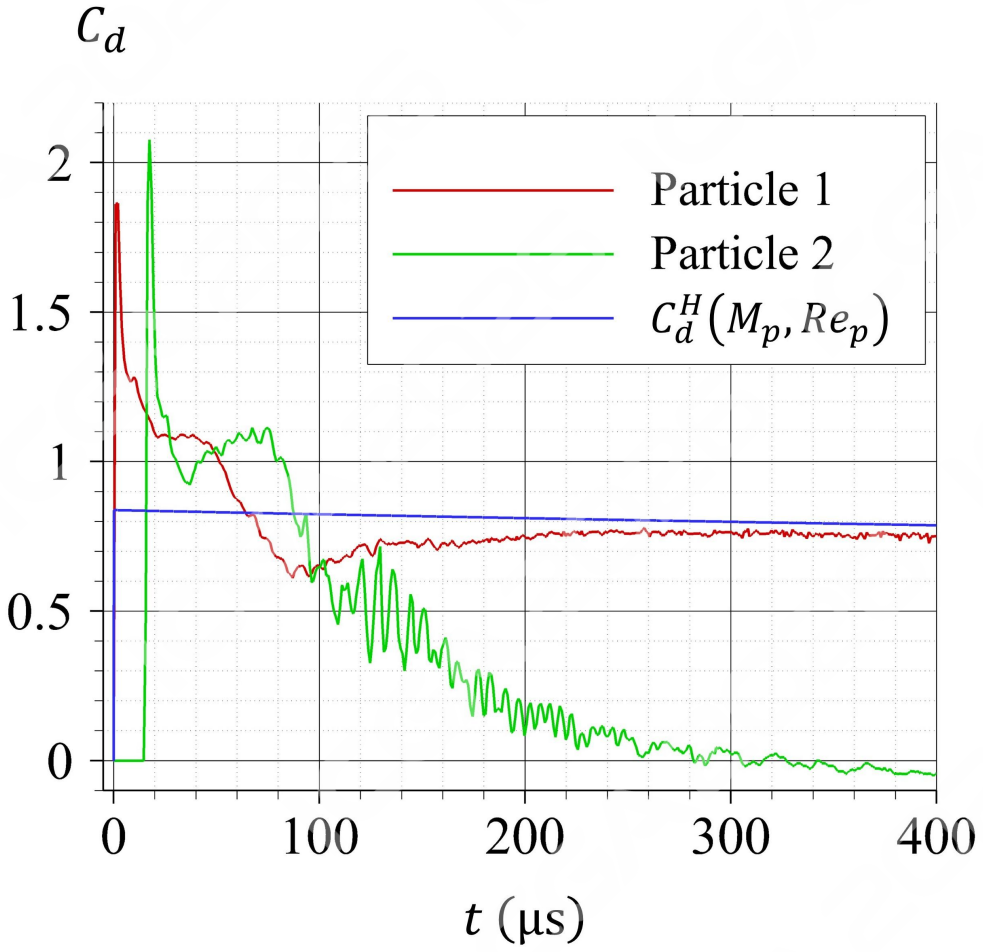
Utkin P.S. et al. Dynamics of motion of a pair of particles in a supersonic flow // Shock Waves. 2021. 6.

Introduction

Unsteady aerodynamic effects



Whalen T.J., Laurence S.J. // JFM. 2026.



C_d from simulations:

$$C_d = \frac{F_z}{\frac{1}{2}\rho_{SW}(u_{SW} - u_p)^2 \frac{\pi d^2}{4}}$$

C_d from analytics:

$$\begin{cases} \dfrac{dx_p}{dt} = u_p \\ \dfrac{du_p}{dt} = \dfrac{3}{4}\dfrac{\rho_{SW}}{\rho_p}\dfrac{|u_{SW} - u_p|}{d} C_d^H(M_p, Re_p)(u_{SW} - u_p) \end{cases}$$

Henderson C.B. // AIAA J. 1976. 6.

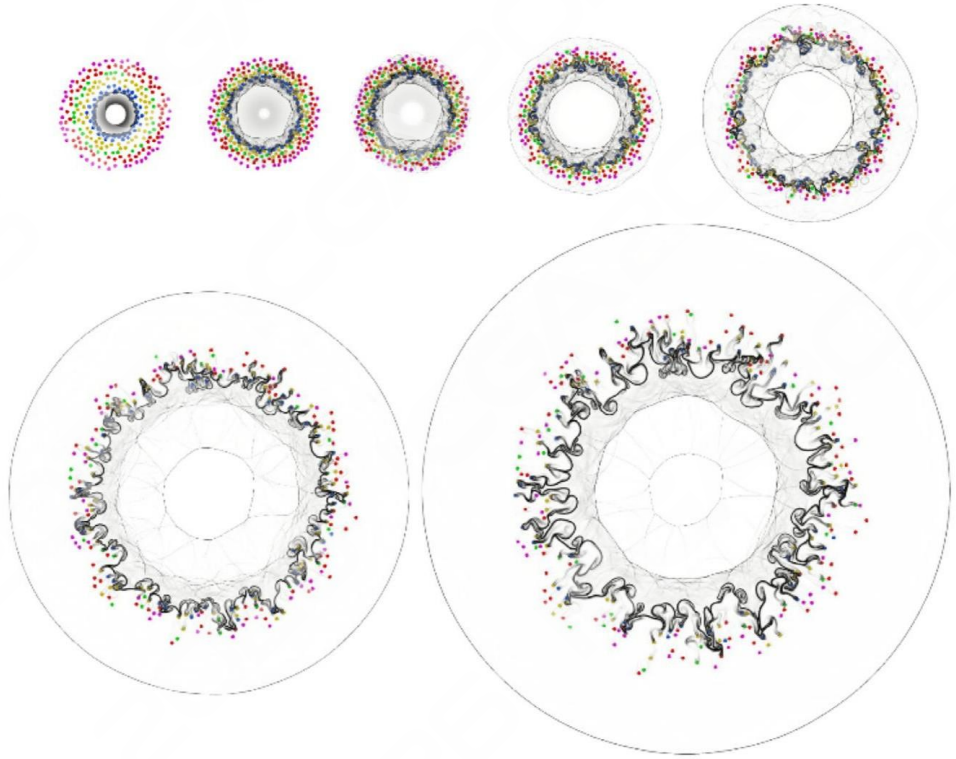
$$M_p = \frac{|u_{SW} - u_p|}{c_{SW}} \qquad Re_p = \frac{\rho_{SW}|u_{SW} - u_p|d}{\mu}$$

Utkin P.S. et al. Dynamics of motion of a pair of particles in a supersonic flow // Shock Waves. 2021. 6.

Introduction

Particle–resolved simulations

To account for the effects discussed above, simulations that resolve individual particles are needed. Of particular interest are studies of particle motion and collisions in high-speed compressible flows. However, new numerical methods of this kind are presented regularly, but much fewer studies use them to investigate real physical processes. In these studies, particle density is often set unrealistically low to make particles move faster under gas-pressure forces and reduce computational costs. For example, in this impressive simulation of explosive dispersal using the method described in the first reference, the particle density was only twice the density of the surrounding gas. In reality, it should have been at least several hundred times higher. This simplification can lead to particle motion that is very different from what we would expect for particles with realistic masses.

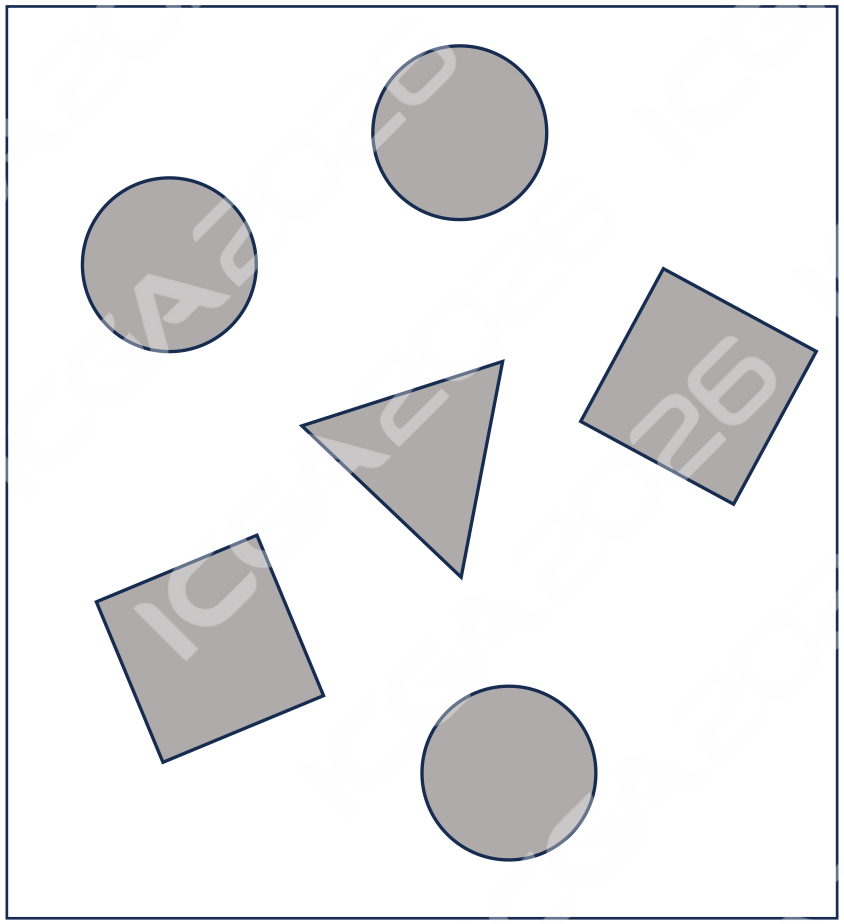


From Young C.J. et al. // Int. J. Multiphase Flow. 2025.

- Mehta Y., Goetsch R.J., Vasilyev O.V., Regele J.D. A particle resolved simulation approach for studying shock interactions with moving colliding solid particles // Comp. Fluids. 2022. 248.
- Meng B., Zeng J., Li S., Tian B., Liu J. A particle-resolved direct numerical simulation method for the compressible gas flow and arbitrary shape solid moving with a uniform framework // Comp. Phys. Commun. 2024. 303.
- Liu Q. et al. Ad adaptive direct-forcing immersed boundary method with subcycled time advancement for compressible flows over irregular solid boundaries // Phys. Fluids. 2026. 38.

Mathematical model

2D Euler equations are solved in a rectangular computational domain of fixed size with moving/stationary boundaries corresponding to moving particles



Hard-sphere model for particle collisions

Equations describing gas behavior

$$\frac{\partial \mathbf{u}}{\partial t} + \frac{\partial \mathbf{f}}{\partial x} + \frac{\partial \mathbf{g}}{\partial y} = \mathbf{0}$$

$$\mathbf{u} = \begin{bmatrix} \rho_g \\ \rho_g u_g \\ \rho_g v_g \\ e_g \end{bmatrix} \quad \mathbf{f} = \begin{bmatrix} \rho_g u_g \\ \rho_g u_g^2 + p_g \\ \rho_g u_g v_g \\ u_g(e_g + p_g) \end{bmatrix} \quad \mathbf{g} = \begin{bmatrix} \rho_g v_g \\ \rho_g u_g v_g \\ \rho_g v_g^2 + p_g \\ v_g(e_g + p_g) \end{bmatrix}$$

$$e_g = \frac{\rho_g}{2}(u_g^2 + v_g^2) + \frac{p_g}{\gamma_g - 1}$$

Equations of motion for a particle

$$\frac{dx_p}{dt} = u_p \quad \frac{dy_p}{dt} = v_p \quad \frac{d\alpha_p}{dt} = \omega_p$$

$$m_p \frac{du_p}{dt} = F_x \quad m_p \frac{dv_p}{dt} = F_y \quad J_p \frac{d\omega_p}{dt} = T_z$$

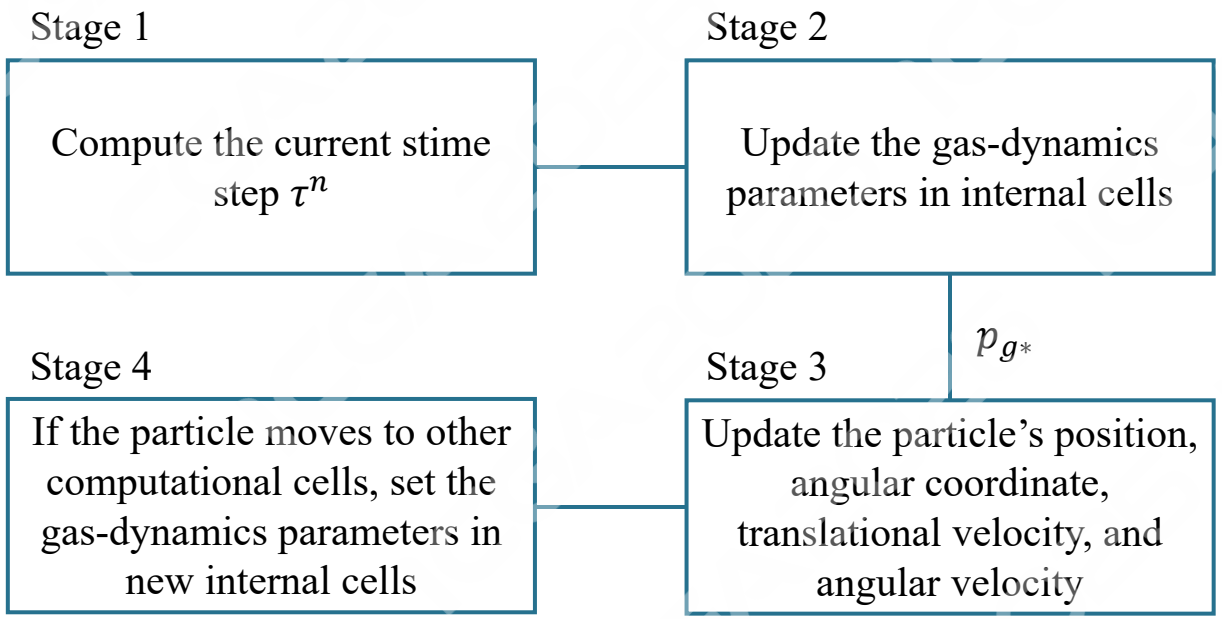
$$\mathbf{F} = \oint p_{g*}(\mathbf{r}_b)\,\mathbf{n}\,dl \quad T = \oint p_{g*}(\mathbf{r}_b)\,(\mathbf{r}_b - \mathbf{r}_p) \times \mathbf{n}\,dl$$

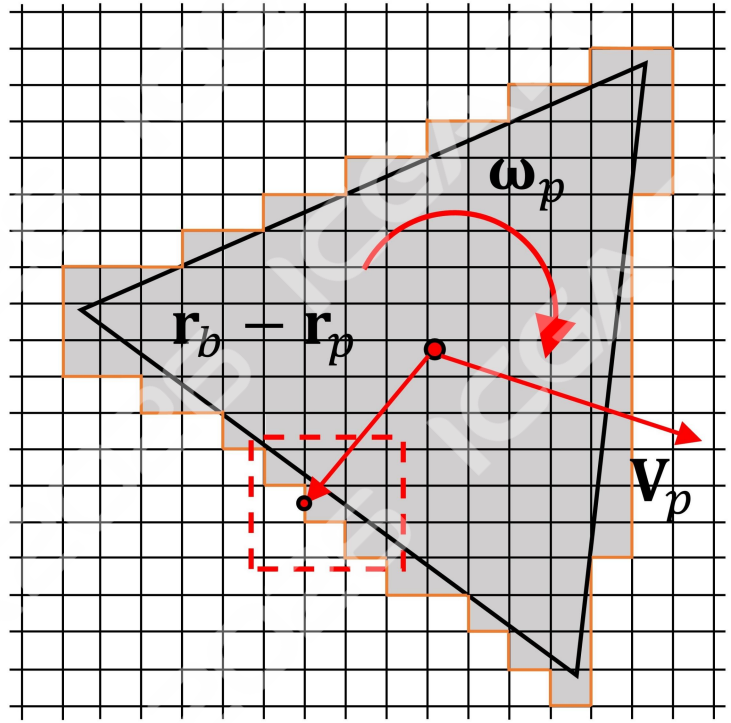
Numerical method

An interface tracking method

- The computational domain was discretized into Cartesian square cells with uniform spacing h in both spatial directions.
- At each discrete time level, there were two types of cells: internal (entirely inside the fluid domain) and external (either entirely inside a body or intersected by a body boundary). The numerical solution was evolved only in internal cells.

One-step algorithm





- Chertock A. et al. // ESAIM: M2AN. 2008.
- Chertock A., Kurganov A. // Comm. Math. Sci. 2008.

Numerical method

An interface tracking method

1

$$\mathbf{U}_{i,j}^{n} = \begin{bmatrix} (\rho_g)_{i,j}^{n} \\ (\rho_g)_{i,j}^{n}(u_g)_{i,j}^{n} \\ (\rho_g)_{i,j}^{n}(v_g)_{i,j}^{n} \\ (e_g)_{i,j}^{n} \end{bmatrix}$$

2

$$\mathbf{U}_{ghost} = \begin{bmatrix} (\rho_g)_{i,j}^{n} \\ (\rho_g)_{i,j}^{n}\left(2u_b^n - (u_g)_{i,j}^{n}\right) \\ (\rho_g)_{i,j}^{n} v_b^n \\ \frac{(\rho_g)_{i,j}^{n}}{2}\left(\left(2u_b^n - (u_g)_{i,j}^{n}\right)^2 + (v_b^n)^2\right) + \frac{(p_g)_{i,j}^{n}}{\gamma_g - 1} \end{bmatrix}$$

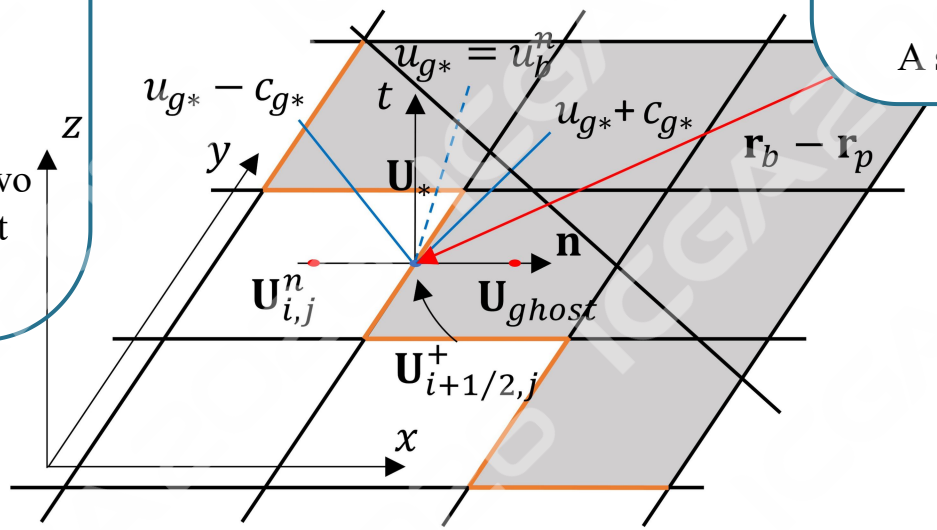
A solid-wall extrapolation of the solution in cell (i, j)

3

$$\mathbf{U}_* = \begin{bmatrix} \rho_{g*} \\ \rho_{g*} u_b^n \\ \rho_{g*} v_{g*} \\ \frac{\rho_{g*}}{2}\left((u_b^n)^2 + (v_{b*})^2\right) + \frac{p_{g*}}{\gamma_g - 1} \end{bmatrix}$$

$$v_{g*} = \begin{cases} (v_g)_{i,j}^{n}, & \text{if } u_b^n \geq 0, \\ v_b^n, & \text{if } u_b^n < 0. \end{cases}$$

The interpolation between these two states is carried out using the exact solution of the Riemann problem.



4

$$\mathbf{U}_{i+1/2,j}^{+} = \begin{cases} \mathbf{U}_{ghost}, & \text{if } u_{g*} + c_{g*} < 0, \\ \mathbf{U}_*, & \text{if } -c_{g*} < u_{g*} < c_{g*}, \\ \mathbf{U}_{i,j}^{n}, & \text{if } u_{g*} - c_{g*} > 0. \end{cases}$$

The right state for the numerical flux calculation is taken from the three-wave configuration.

A Godunov-type finite volume scheme was used for spatial discretization, while an explicit Euler scheme was applied for time integration:

$$\mathbf{U}_{i,j}^{n+1} = \mathbf{U}_{i,j}^{n} - \frac{\tau^n}{h}\left(\mathbf{F}_{i+1/2,j} - \mathbf{F}_{i-1/2,j}\right) - \frac{\tau^n}{h}\left(\mathbf{G}_{i,j+1/2} - \mathbf{G}_{i,j-1/2}\right)$$

$$\mathbf{F}_{i+1/2,j} = \mathbf{F}_{St.-Warm.}\left(\mathbf{U}_{i+1/2,j}^{-}, \mathbf{U}_{i+1/2,j}^{+}\right)$$

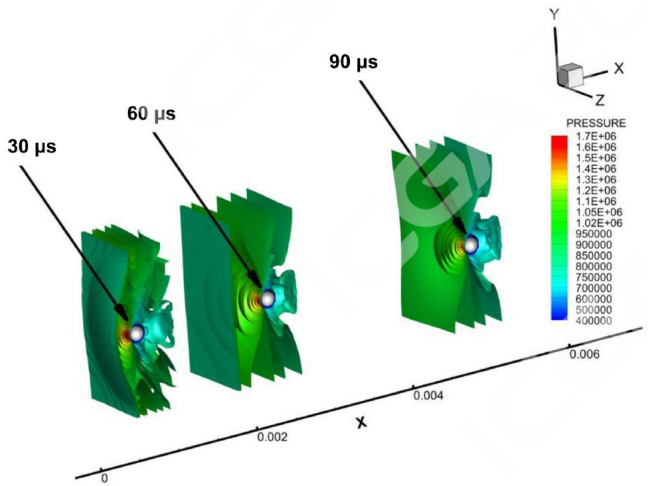
MUSCL reconstruction with the minmod limiter

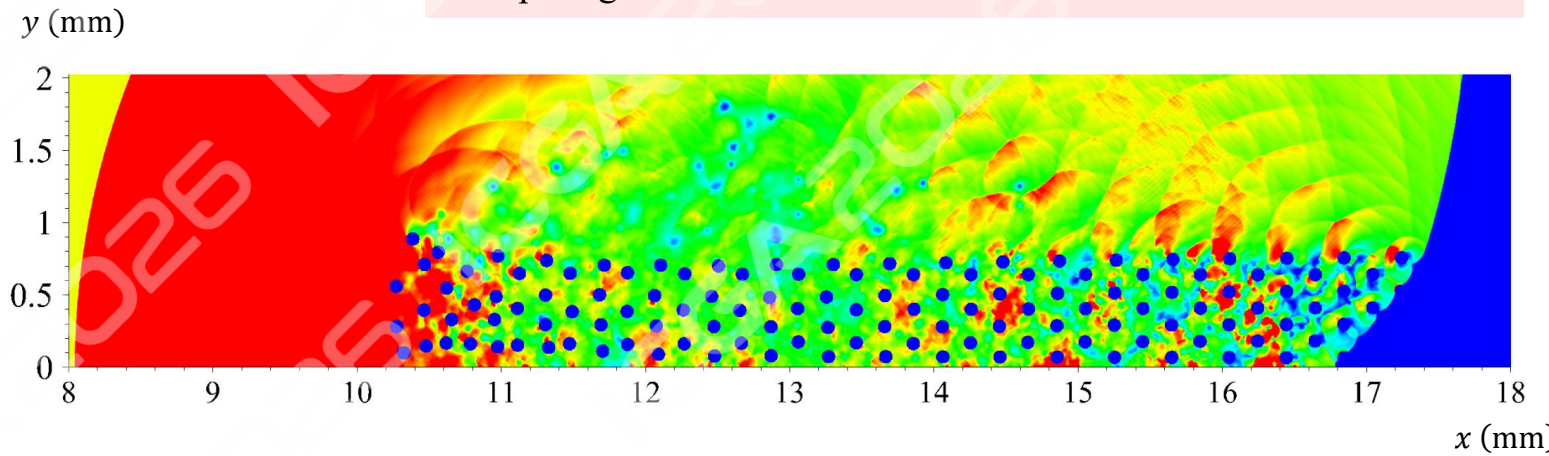
Numerical method

An interface tracking method. Pros and cons.

- The formal order of accuracy of the algorithm for smooth solutions is first order in time and second order in space due to the minmod reconstruction of conservative variable vectors. But the boundary cell treatment procedure utilized only $O(h)$-accurate information about the boundary location, rather than the exact position. Consequently, **the overall accuracy of the method cannot exceed first order**.
- **The boundary treatment is not conservative.** This is due to the lack of an exact determination of the body boundary position within a cell and the method used to determine the gas parameters in newly emerging internal cells. However, the conservation error is confined to the boundary surface, which has codimension one. Therefore, the total conservation error is expected to scale with the mesh size.

- The algorithm is relatively **simple to implement** and does not require solving the problem of determining the shape or square of the intersection of the body boundary with a regular computational cell. This is particularly important when extending the algorithm to three dimensions and considering a system of many interacting particles.
- **Robustness.** Simulations with thousands of particles run smoothly for hundreds of thousands of time steps.
- Domain decomposition **parallelization**, MPI. Grids up to 10^9 cells, up to 2000 processors. The calculations presented below were performed on the BSCC-M9S cluster at the Beijing Super Cloud Computing Center.





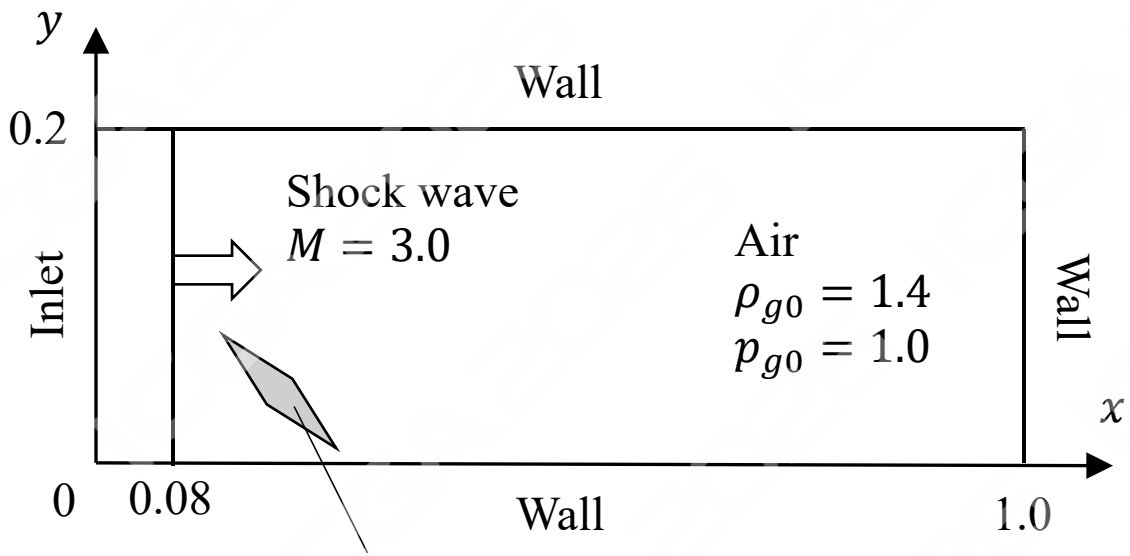
Elesin V.V. et al. // Int. J. Comp. Meth. 2021. 4.

Sidorenko D.A., Utkin P.S. // Comb. Expl. 2020. 13.

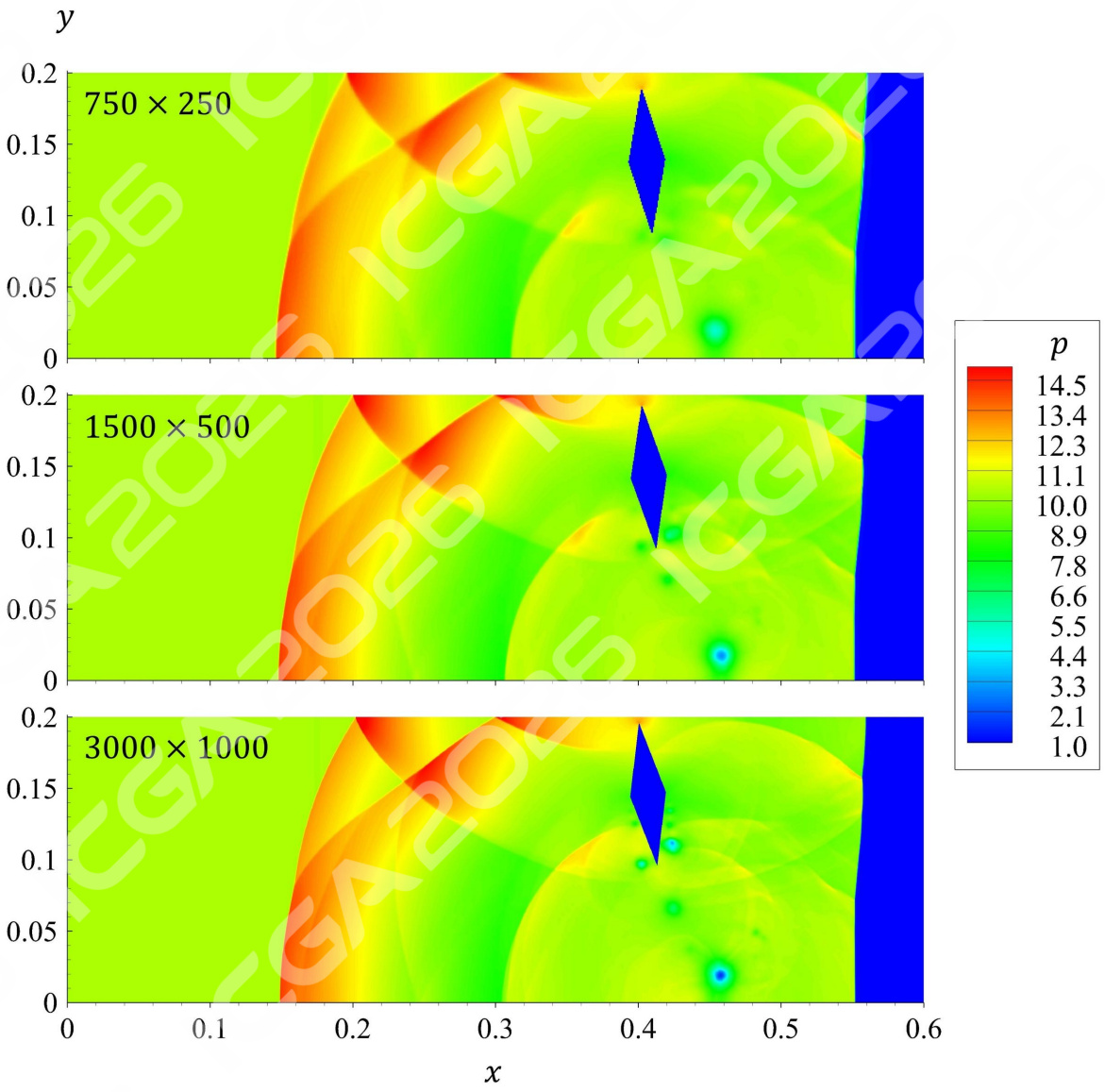
Validation

Liftoff of a diamond-shaped particle

- Test from (Grétarsson J.T. et al. // J. Comp. Phys. 2011) and (Ren Y. et al. // J. Comp. Phys. 2021).
- All quantities are dimensionless.



- $(x_{p0}; y_{p0}) = (0.15; 0.05)$
- $\rho_p = 10.77$
- Major diagonal 0.1, minor diagonal 0.025
- Initial tilt angle of the particle 45°



Validation

Liftoff of a diamond-shaped particle

Estimation of the observed order of convergence of the numerical scheme

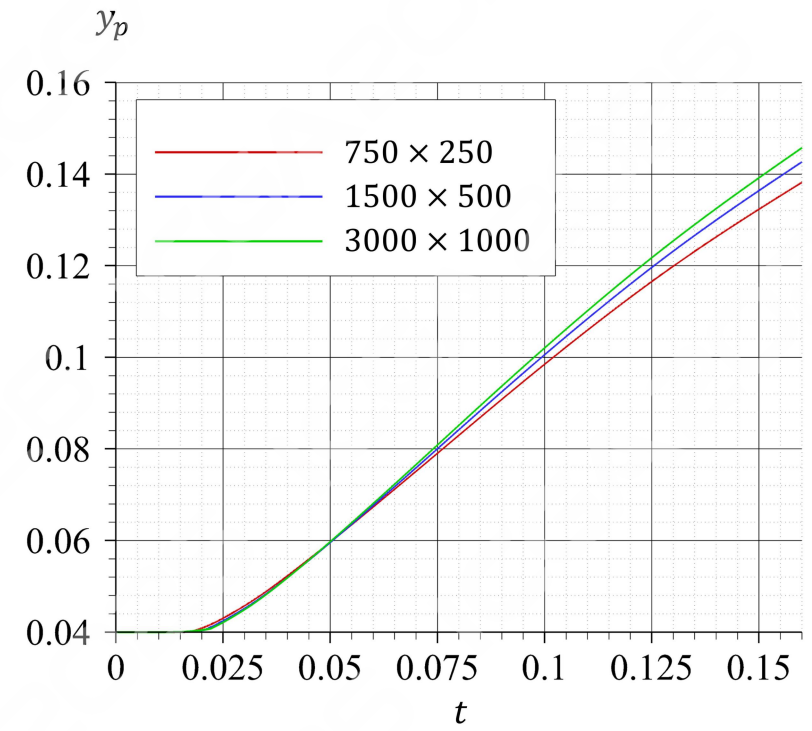
Cell size, h	y_p		v_p		α_p		Total gas mass, m	
	ε_h	p	ε_h	p	ε_h	p	ε_h	p
$8.0\cdot10^{-4}$	$4.457\cdot10^{-3}$	**0.54**	$3.949\cdot10^{-2}$	**0.45**	$3.565\cdot10^{-2}$	**0.40**	$9.5\cdot10^{-5}$	**1.08**
$4.0\cdot10^{-4}$	$3.068\cdot10^{-3}$		$2.893\cdot10^{-2}$		$2.708\cdot10^{-2}$		$4.5\cdot10^{-5}$	
$2.0\cdot10^{-4}$	–		–		–		–	

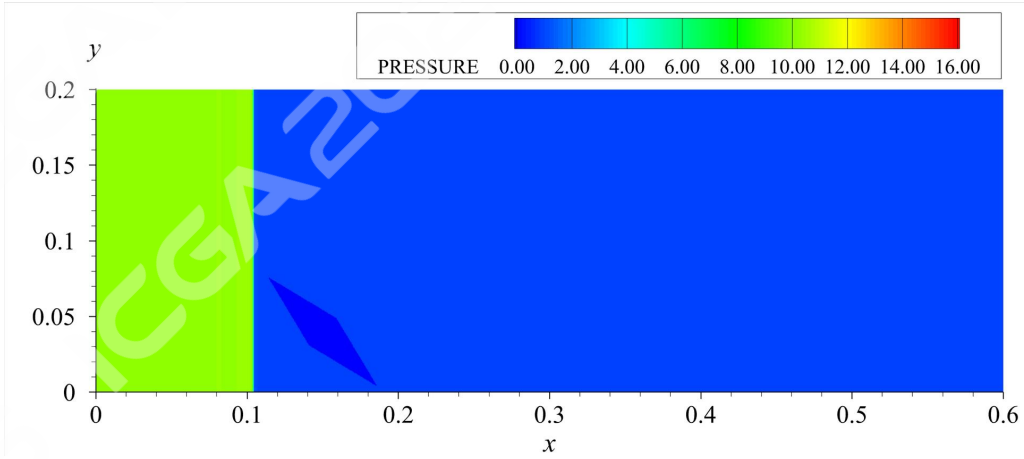
$$\varepsilon_h = \|\xi_h - \xi_{h/2}\|_\infty = \max|\xi_h - \xi_{h/2}|$$

$$p = \log_2 \frac{\varepsilon_h}{\varepsilon_{h/2}}$$

The variable ξ considered were y_p, v_p, α_p, and m

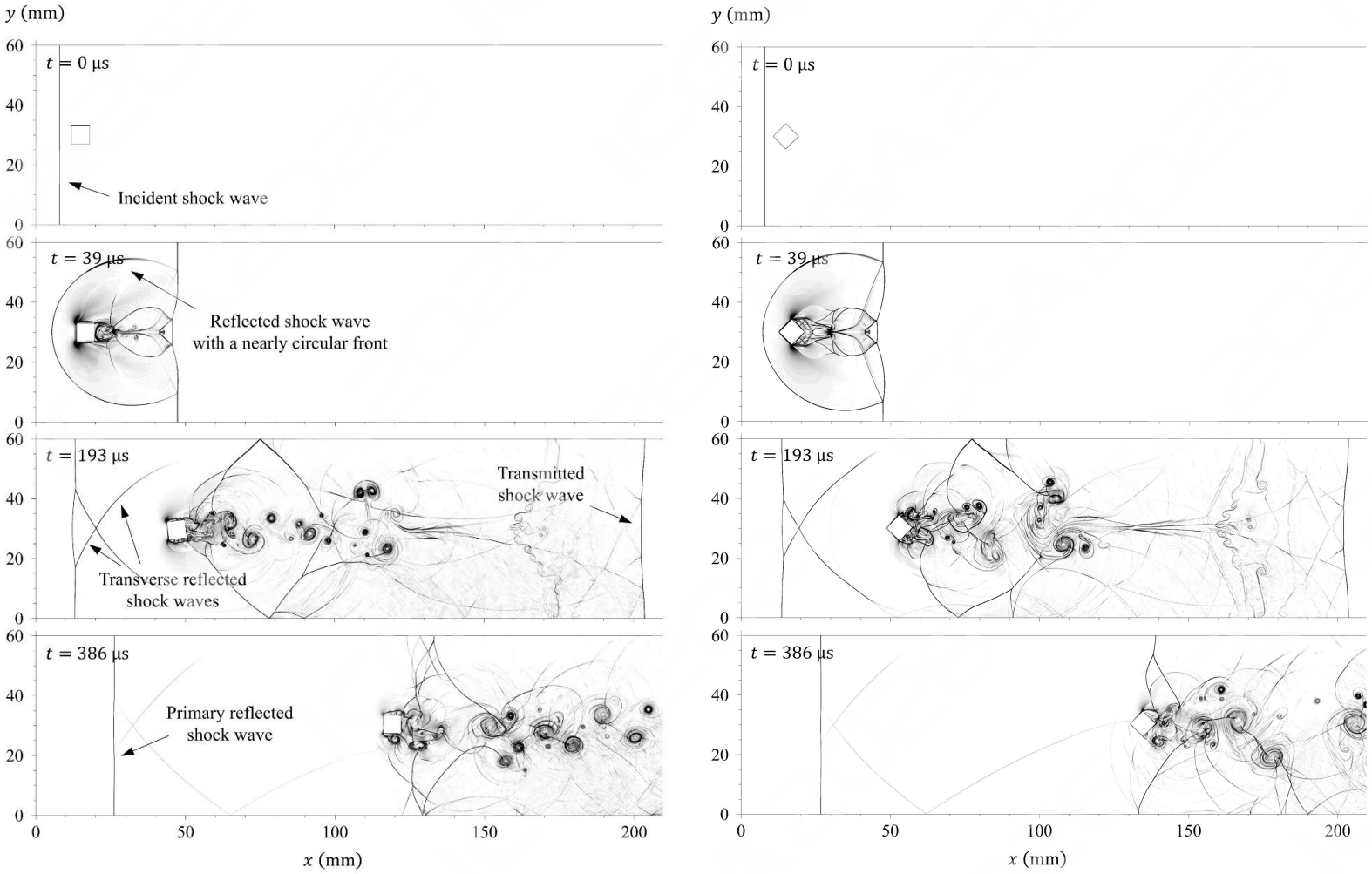
The convergence rates estimated from physical quantities are approximately 0.4–0.5, which is typical for unsteady problems involving shock waves and vortical structures. The relative error in the total gas mass in the system averages approximately 0.03%.

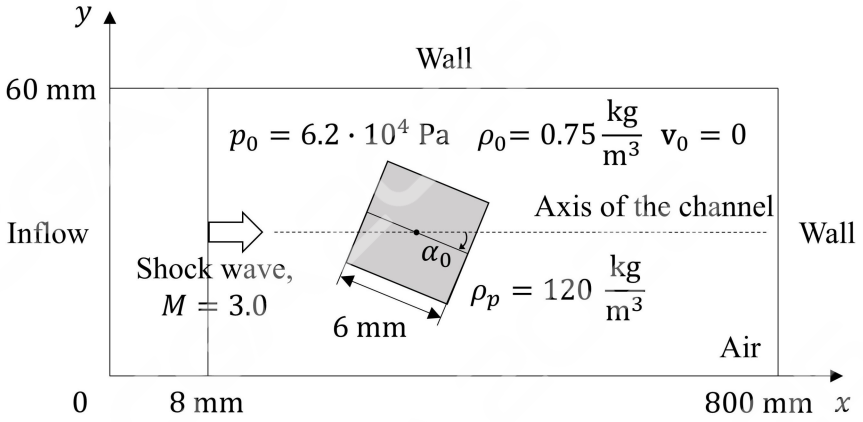




Previous studies

Motion of a square particle in the supersonic flow





The statement follows Boiko V.M., Poplavskii, S.V. // Comb. Expl. Shock Waves. 2005. 41.

If the square particle is initially oriented with its diagonal aligned with the flow, it maintains this position for an order of magnitude longer than when initially positioned with one of its sides perpendicular to the flow. If the initial orientation falls between these two cases, the particle undergoes oscillations that are nearly harmonic. Over time, these oscillations transition into continuous rotation with a constant average angular velocity.

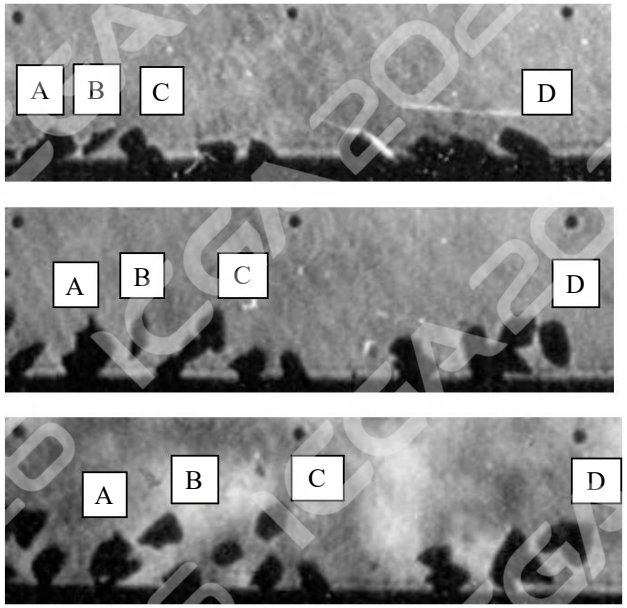
Utkin P., Lopato A. // Europ. Phys. J. Spec. Topics. 2026.

Statement of the problem

Experimental data

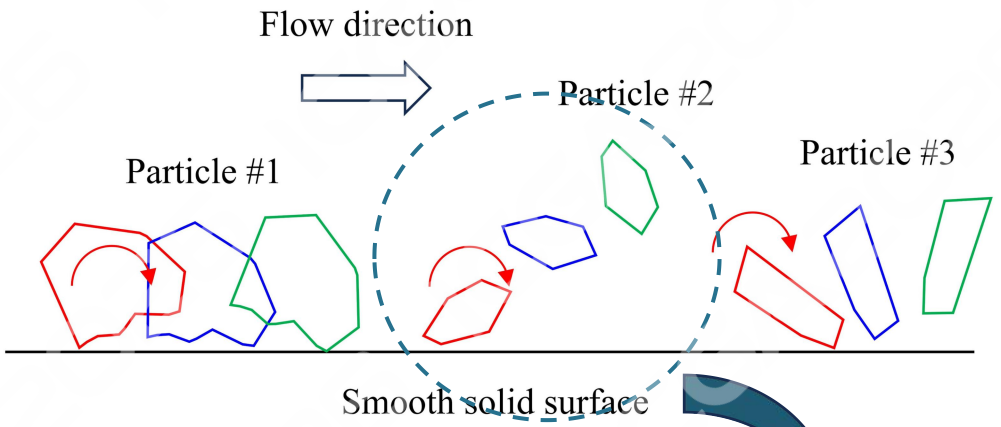
The figure presents frames from a series of shadowgraph images of a dilute monolayer of coal particles behind a shock wave. The particles exhibit different behaviors due to differences in their mass and shape.

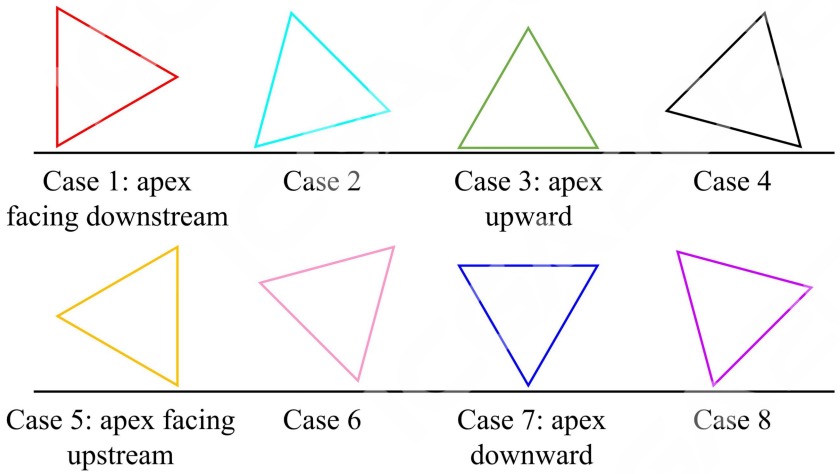
Particle A rolls along the surface but does not detach from the wall even after 450 μs. Particles B and C rotate in the direction of rolling and lift off with velocities of 5–7.5 m/s. No rolling stage is captured for these particles; however, it is observed for particle D: in the top frame, particle D rolls under the action of the flow, while in the subsequent frames it lifts off with a vertical velocity of approximately 6 m/s.

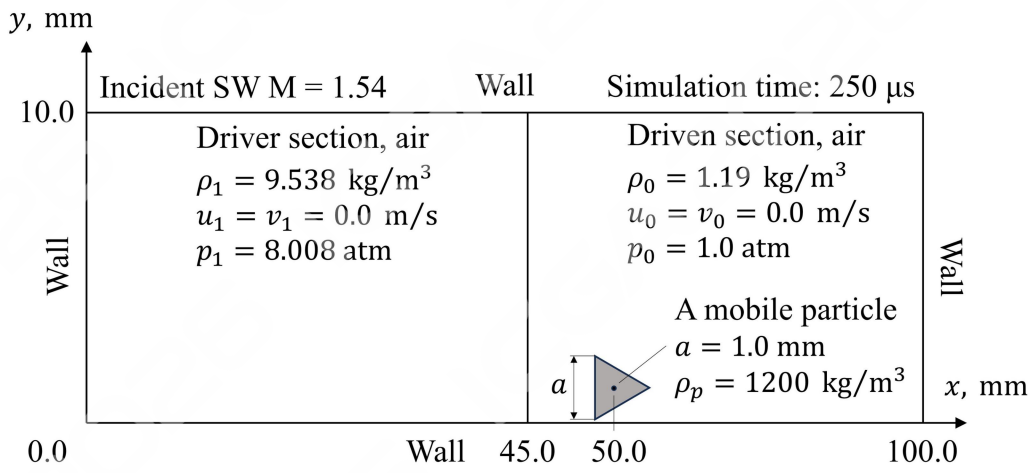


Poplavski S.V. // J. Phys.: Conf. Ser. 2018. 1128.

Schematic illustration of typical scenarios



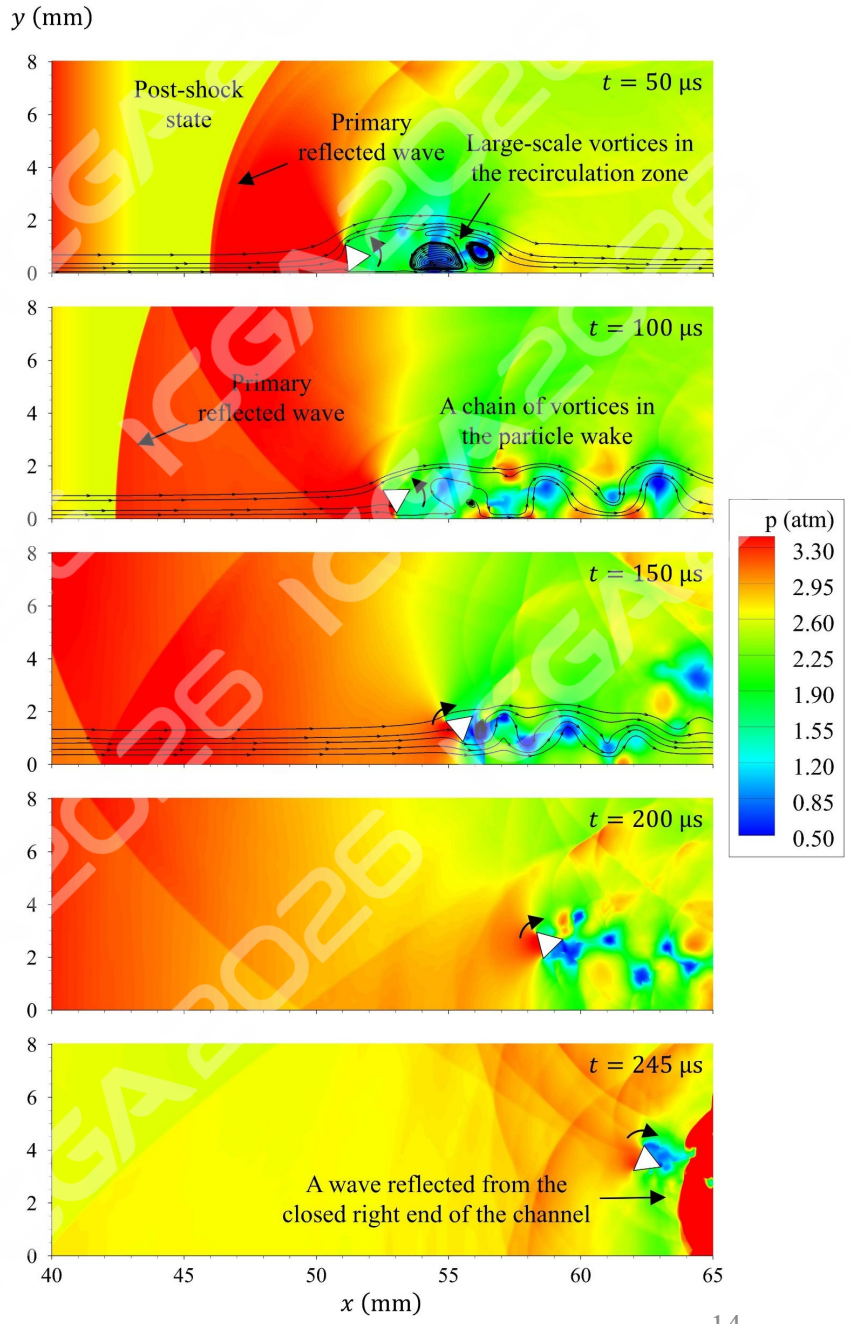




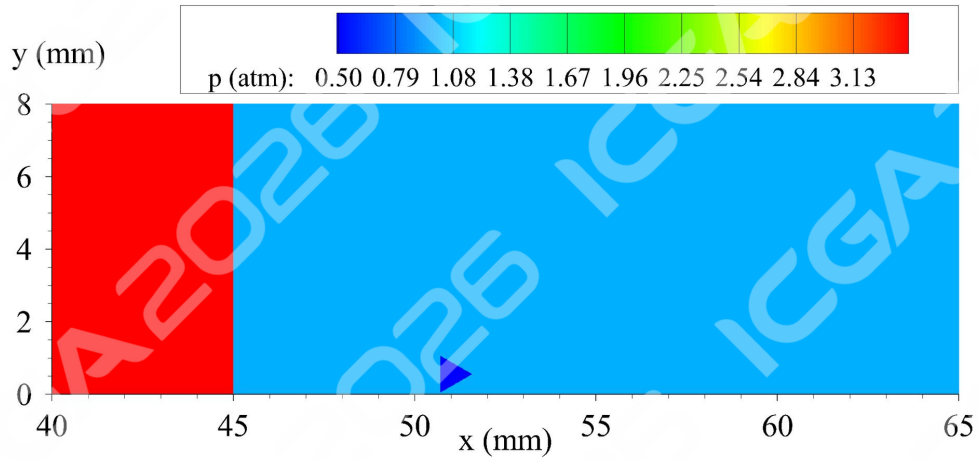
Typical flow patterns

- At the early stage following the interaction of the leading shock wave with the particle, a typical wave pattern develops, including: (1) the primary wave reflected from the particle; (2) several additional reflected waves generated by the interaction of the diffracted shock wave with the surface; and (3) the transmitted wave.
- Large-scale vortices form behind the particle, with diameters comparable to the particle diameter.
- The particle lift-off is caused by the formation of a high-pressure region between the particle and the surface.
- At the later stage, when the particle rises to a certain height, this effect weakens. The particle then continues to move horizontally as it would in a free flow, while its vertical velocity component remains nearly constant.

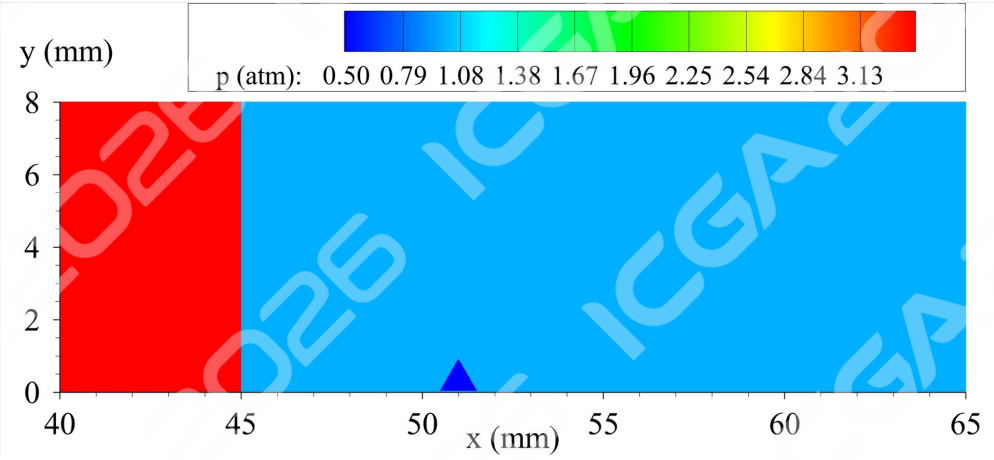
Grid resolution: 100 cells per triangle side, i.e. $h = 10^{-2}$ mm.



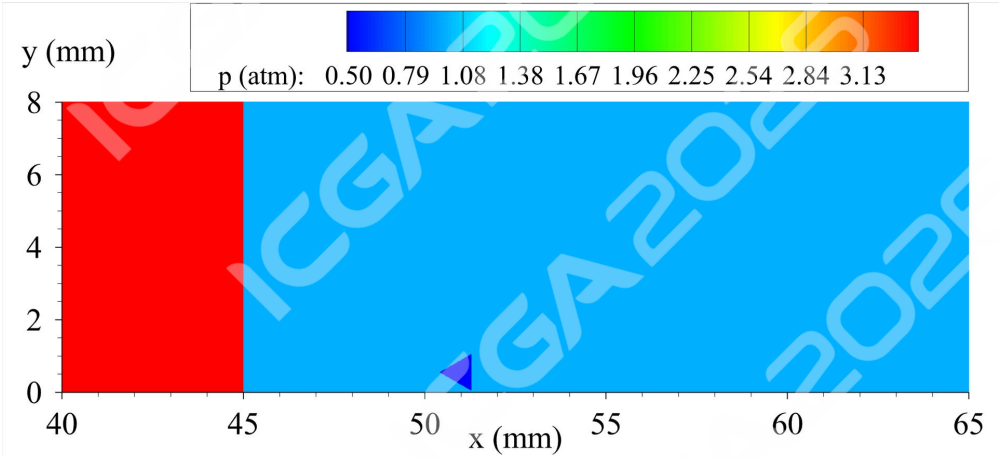
Effect of the initial particle orientation on its lift-off dynamics



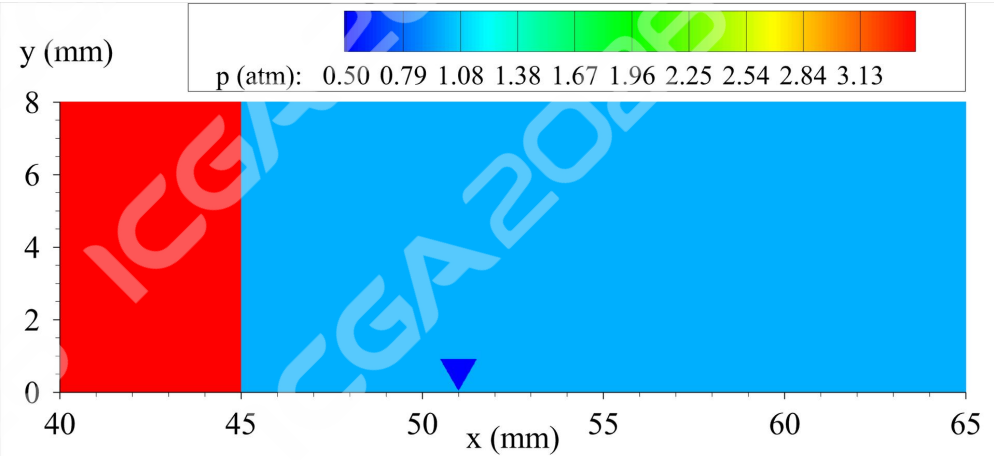
Case 1. Apex facing downstream.



Case 3. Apex upward.

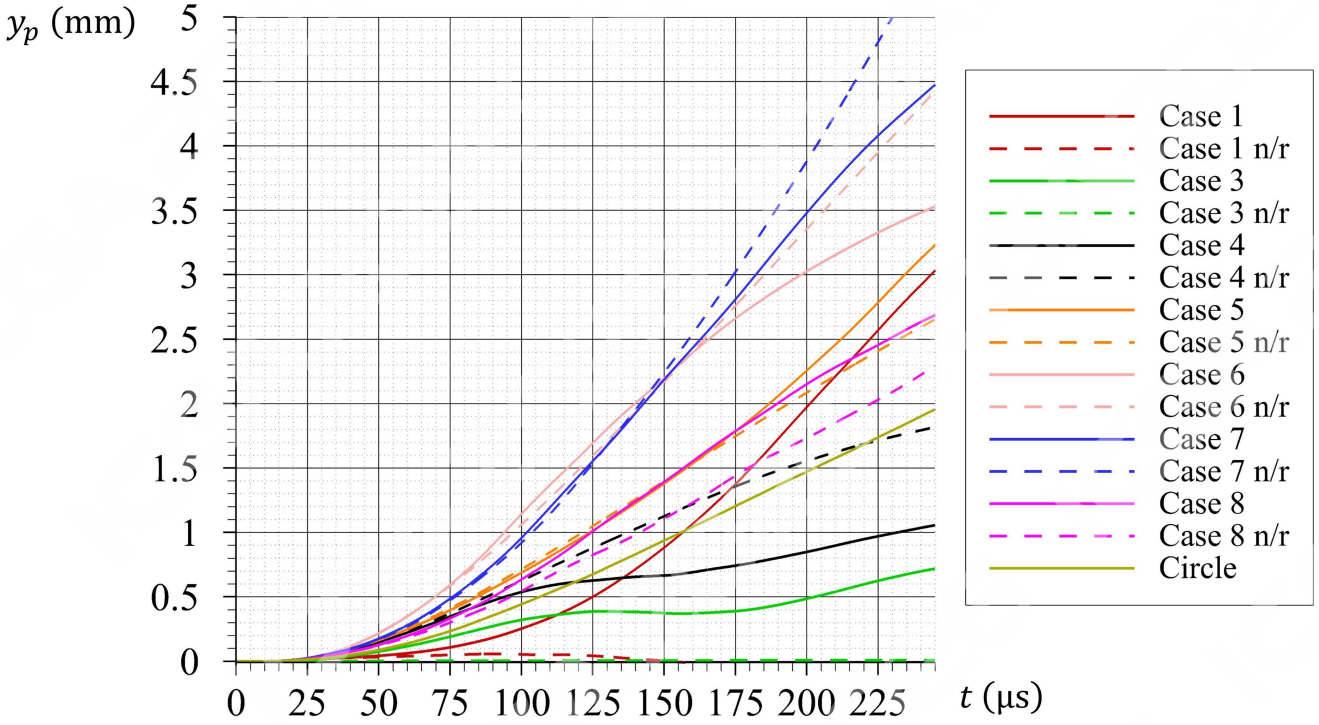


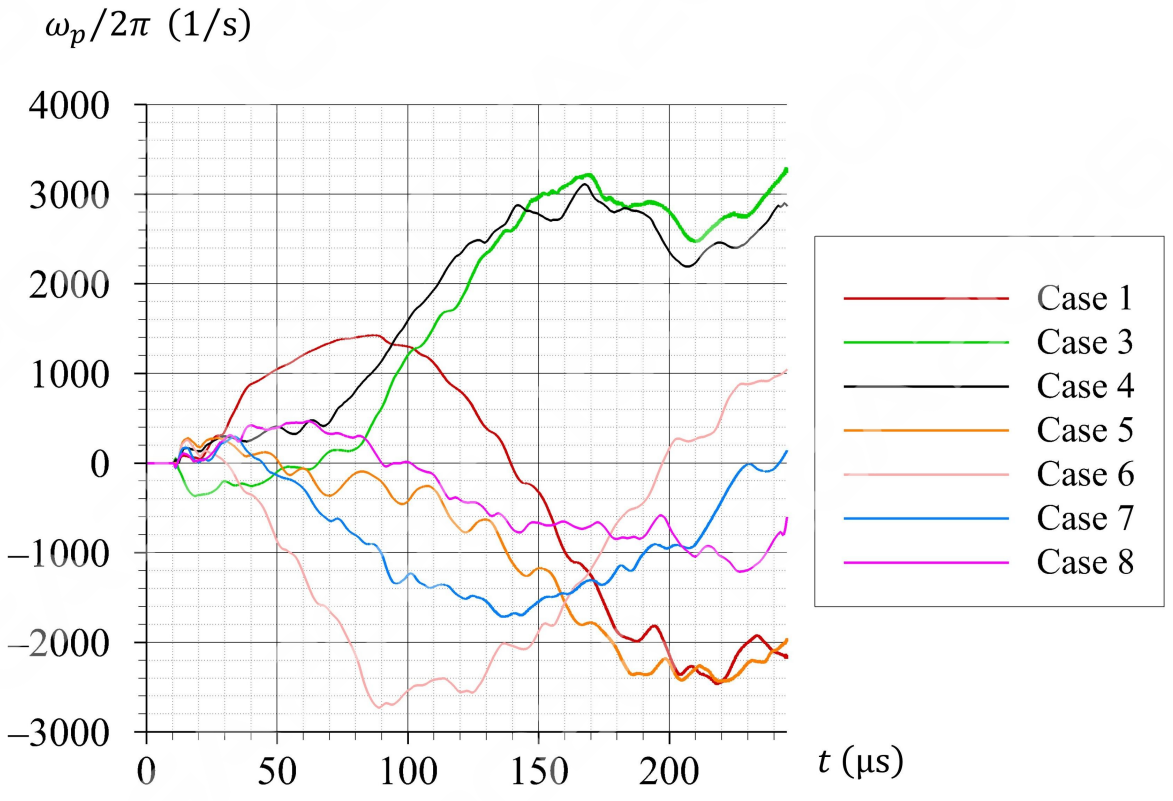
Case 5. Apex facing upstream.

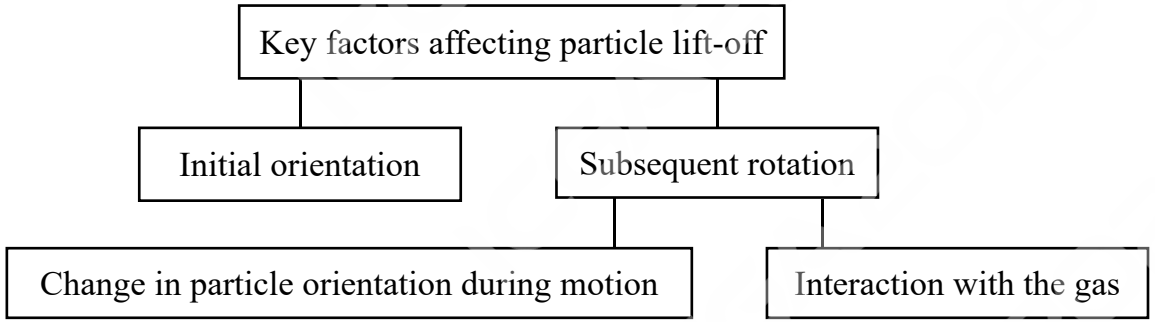


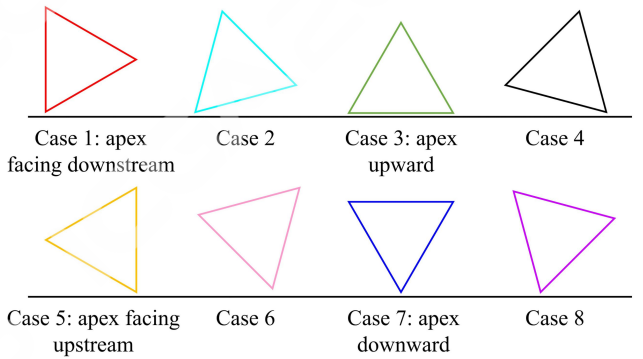
Case 7. Apex downward.

Effect of particle rotation on its lift-off dynamics

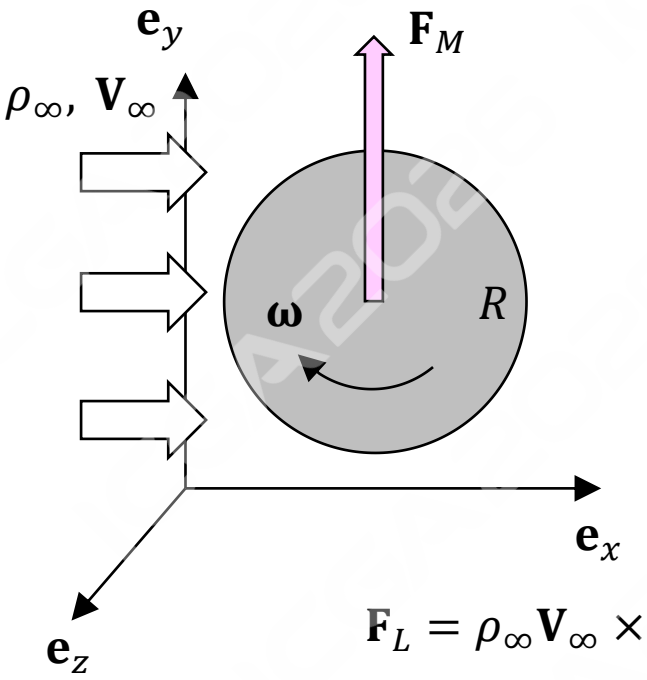








Magnus effect



Kutta–Joukowski theorem. For steady two-dimensional potential flow of an ideal fluid around a stationary body, assuming inviscid and incompressible flow with freestream velocity $\mathbf{V}_\infty$ and density ρ_∞, the transverse force per unit length of the body in the presence of circulation Γ is given by the following expression:

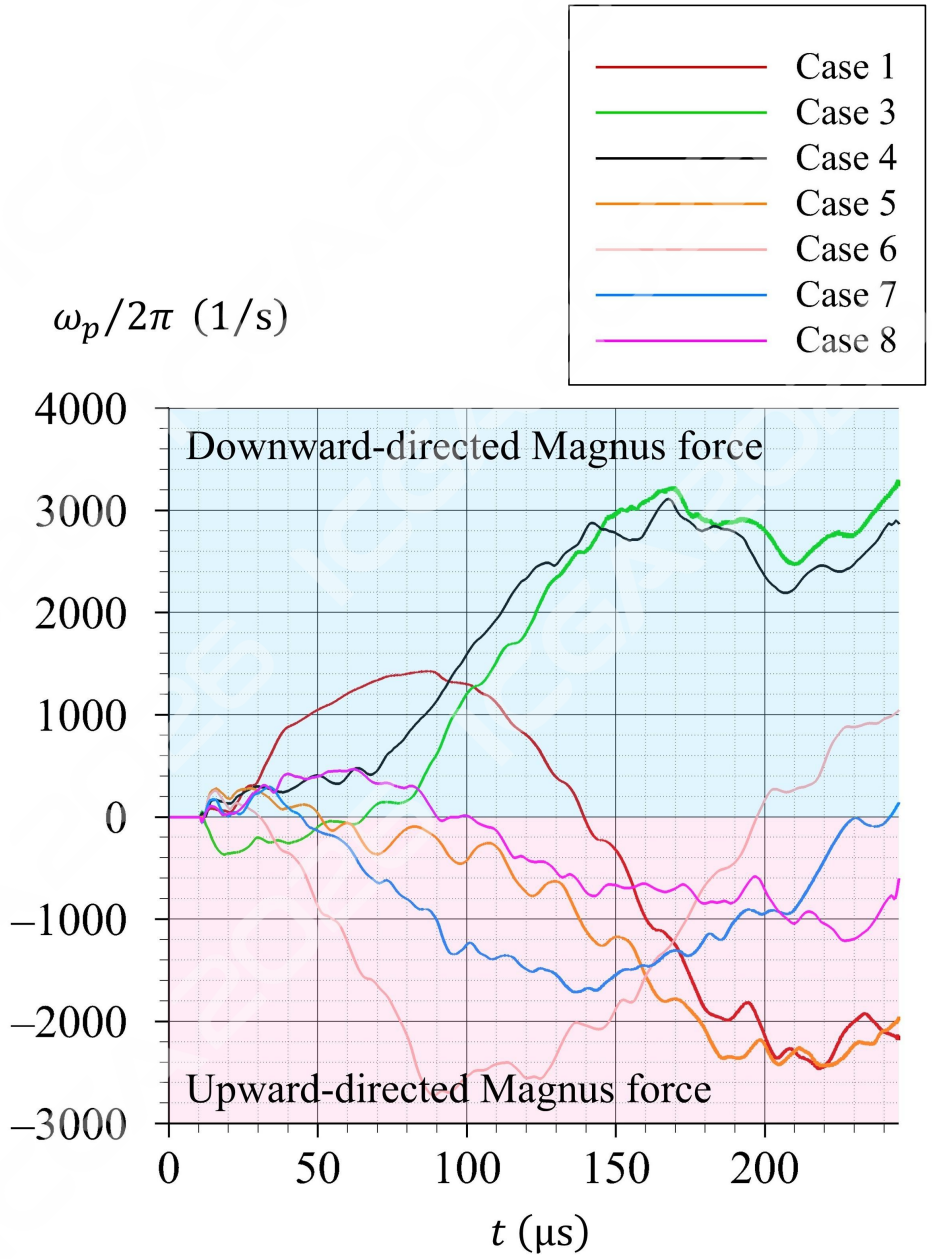
$$\mathbf{F}_L = \rho_\infty \mathbf{V}_\infty \times (\Gamma \mathbf{e}_z), \qquad \Gamma = \oint_C \mathbf{V}_g \cdot d\mathbf{l}\,.$$

For a rotating cylinder, the classical idealized model relates the circulation to the angular velocity vector as follows:

$$\Gamma \mathbf{e}_z = 2\pi R^2 \boldsymbol{\omega},$$

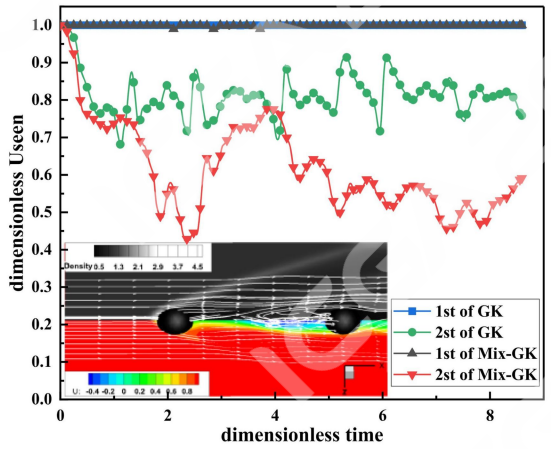
from where:

$$\mathbf{F}_M = 2\pi R^2 \rho_\infty \mathbf{V}_\infty \times \boldsymbol{\omega}.$$

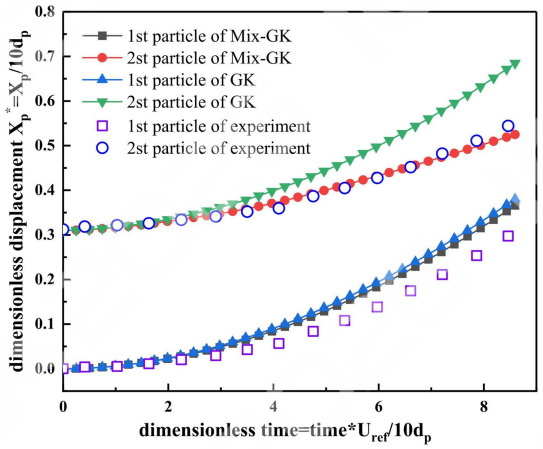


How can these results be used in simulations of real–world applications?

Recently, our findings (Utkin P.S. et al. // Shock Waves. 2021. 31) were utilized in (Yang X. et al. // Int. J. Multiphase Flow. 2024. 170) to justify a two-phase Euler–Lagrangian model based on the particle-in-cell method with a Gaussian kernel. The Euler–Lagrangian model enables accurate tracking of arbitrarily sized spherical particles in supersonic flows by correctly accounting for the effects of shock waves on particle drag. The current work extends our previous study to complex-shaped bodies and, similarly, can contribute to the development of reduced-order models for two-phase flows.

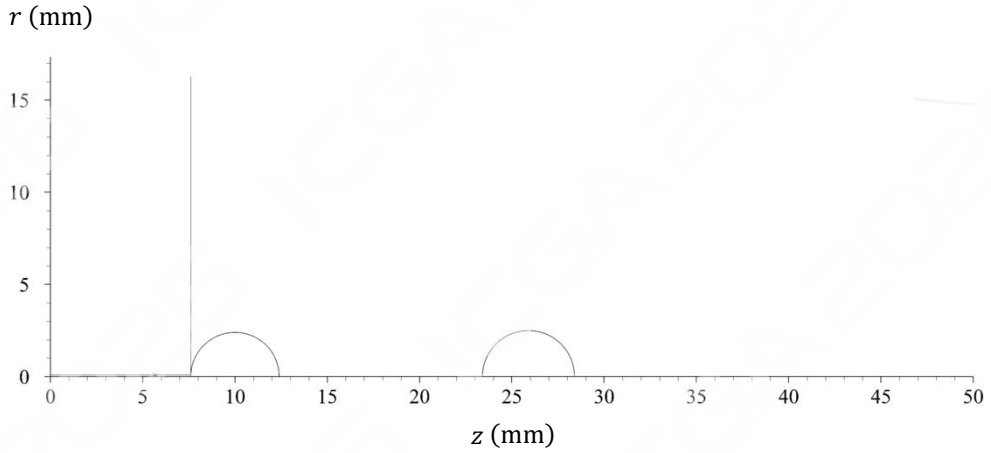


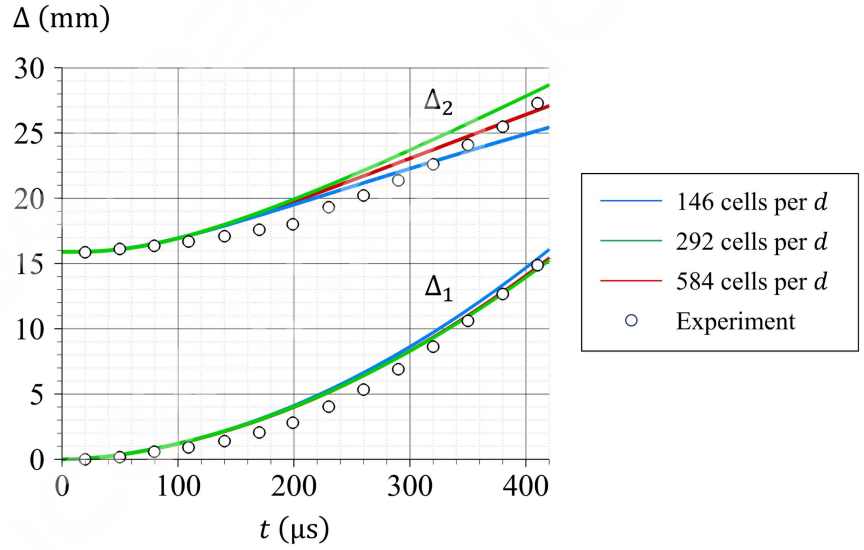
(a) u_{seen} exerting on particles



(b) X_p compared with Utkin(Utkin et al., 2021) experiment

Yang X. et al. // Int. J. Multiphase Flow. 2024.





Utkin P.S. et al. // Shock Waves. 2021.

Thank you for your kind attention!
非常感谢您的关注！
Спасибо за внимание!

Pavel Utkin

Harbin Institute of Technology
School of Astronautics
International Center for Applied Mechanics

Email: utkin@hit.edu.cn

Physics of Fluids ARTICLE pubs.aip.org/aip/pof

Effect of particle shape on lift-off from a surface behind a shock wave

Cite as: Phys. Fluids **38**, 113312 (2026); doi: 10.1063/5.0348677
Submitted: 17 June 2026 · Accepted: 28 October 2026 ·
Published Online: 12 November 2026

Zhao Liu (刘钊),[1] Pavel Utkin (П. Уткин),[1,a)] Alexander Lopato (А. Лопато),[2,3] and Fei Jia (贾飞)[1]

AFFILIATIONS

[1]Harbin Institute of Technology, Department of Astronautical Science and Mechanics, No. 92 West Dazhi Street, Nan Gang District, Harbin, Heilongjiang 150001, China
[2]Keldysh Institute of Applied Mathematics of the Russian Academy of Sciences, 4 Miusskaya Square, Moscow 125047, Russia
[3]Sechenov University, 8-2 Trubetskaya str., Moscow 119991, Russia

[a)]Author to whom correspondence should be addressed: utkin@hit.edu.cn

ABSTRACT

We investigate the lift-off dynamics of non-circular particles from a smooth surface in gas–solid flows relevant to dust explosions and shock-driven multiphase systems. Particles of natural and industrial origin often possess irregular shapes, yet the effect of shape on shock-induced lift-off and dispersion remains insufficiently understood. We consider the lift-off of an initially resting triangular particle with a side length of 1 mm in the flow behind a Mach 1.5 shock wave over 250 μs. The problem setup is qualitatively consistent with laboratory experiments on the lift-off of a coal particle. The flow is described by the two-dimensional compressible Euler equations and solved using an interface-tracking method that accounts for the evolving fluid–solid boundary. Eight initial orientations are considered, including apex facing upstream, apex facing downstream, apex upward, apex downward, and four intermediate ones. Results are compared with those for a circular particle of equivalent area. By separating geometric and rotational effects through simulations with and without rotation, we show that the lift-off dynamics is a superposition of two factors—initial orientation of a particle and its rotation. Rotation can either promote or hinder lift-off by changing the particle orientation relative to the flow during its motion and by affecting the flow field around the particle through a pressure-induced Magnus-like effect. An estimate of the contribution of the Magnus force to the lift coefficient is provided based on the averaged angular velocity of the particles and the circulation of the gas velocity along a contour around the particle.

Published under an exclusive license by AIP Publishing. https://doi.org/10.1063/5.0348677

I. INTRODUCTION

Powdered materials of natural or artificial origin are finding increasingly wide application in modern technologies and energy production, including mining, food processing, metal processing, wood processing, and the textile industry. Practical experience has shown that most of these materials are highly explosive. Despite differences in their chemical nature, explosions of various types of dust—not only coal dust, but also aluminum dust,[1] wood dust,[2] and corn starch dust[3]—exhibit similar development patterns and equally destructive consequences. In terms of unpredictability, material damage, and human casualties, dust explosions are recognized as the most dangerous among the man-made disasters of the past two centuries.[4] The continued occurrence of severe accidents involving dispersed combustible materials indicates that the physical mechanisms governing dust explosions are still not fully understood, motivating further studies of the fundamental processes involved.

Shock waves play a central role in the initiation and development of dust explosions because they govern both ignition and explosive-mixture formation in gas–solid systems. Even in situations where a combustible mixture has not been prepared in advance, such as in the presence of deposited dust layers, a propagating shock wave can entrain particles and generate an explosive dust–gas cloud. The entrainment of deposited granular materials behind a shock wave represents a complex multiphase flow problem involving numerous interphase interaction mechanisms. As emphasized by Ugarte *et al.*,[5] existing experimental and numerical studies still report contradictory results regarding the dynamics of dust entrainment. Consequently, a consistent physical description of shock-induced particle entrainment remains unavailable.

The inert stage of shock-wave interaction with a dust–gas mixture constitutes one of the key unresolved aspects of this problem. During this stage, momentum exchange is governed primarily by velocity non-equilibrium between the phases, giving rise to characteristic relaxation